

# UCSF

## UC San Francisco Previously Published Works

### Title

Antibody Probes of Module 1 of the 6-Deoxyerythronolide B Synthase Reveal an Extended Conformation During Ketoreduction

### Permalink

<https://escholarship.org/uc/item/6t27q773>

### Journal

Journal of the American Chemical Society, 142(35)

### ISSN

0002-7863

### Authors

Cogan, Dillon P  
Li, Xiuyuan  
Sevillano, Natalia  
[et al.](#)

### Publication Date

2020-09-02

### DOI

10.1021/jacs.0c05133

Peer reviewed



Published in final edited form as:

*J Am Chem Soc.* 2020 September 02; 142(35): 14933–14939. doi:10.1021/jacs.0c05133.

## Antibody Probes of Module 1 of the 6-Deoxyerythronolide B Synthase Reveal an Extended Conformation During Ketoreduction

Dillon P. Cogan<sup>1</sup>, Xiuyuan Li<sup>1</sup>, Natalia Sevillano<sup>2</sup>, Irimpan I. Mathews<sup>3</sup>, Tsutomu Matsui<sup>3</sup>, Charles S. Craik<sup>2</sup>, Chaitan Khosla<sup>1,4,5,\*</sup>

<sup>1</sup>Department of Chemistry, Stanford University, Stanford, California 94305, United States

<sup>2</sup>Department of Pharmaceutical Chemistry, University of California San Francisco, San Francisco, California 94158, United States

<sup>3</sup>Stanford Synchrotron Radiation Lightsource, SLAC National Accelerator Laboratory, Stanford University, Menlo Park, California 94025, United States

<sup>4</sup>Department of Chemical Engineering, Stanford University, Stanford, California 94305, United States

<sup>5</sup>Department of Stanford ChEM-H, Stanford University, Stanford, California 94305, United States

### Abstract

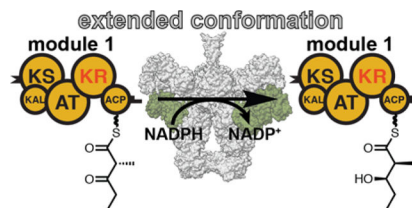
The 6-deoxyerythronolide B synthase (DEBS) is a prototypical assembly-line polyketide synthase (PKS) that synthesizes the macrocyclic core of the antibiotic erythromycin. Each of its six multidomain modules presumably sample distinct conformations, as biosynthetic intermediates tethered to their acyl carrier proteins interact with multiple active sites during the courses of their catalytic cycles. The spatiotemporal details underlying these protein dynamics remain elusive. Here we investigate one aspect of this conformational flexibility using two domain-specific monoclonal antibody fragments ( $F_{ab}$ s) isolated from a very large naïve human antibody library. Both  $F_{ab}$ s, designated 1D10 and 2G10, bound specifically and with high affinity to the ketoreductase domain of DEBS module 1 (KR1). Comparative kinetic analysis of stand-alone KR1 as well as a truncated bimodular derivative of DEBS revealed that 1D10 inhibited KR1 activity whereas 2G10 did not. Co-crystal structures of each KR1- $F_{ab}$  complex provided a mechanistic rationale for this difference. A hybrid PKS module harboring KR1 was engineered, whose individual catalytic domains have been crystallographically characterized at high resolution. Size exclusion chromatography coupled to small-angle X-ray scattering (SEC-SAXS) of this hybrid module bound to 1D10 provided further support for the catalytic relevance of the “extended” model of a PKS module. Our findings reinforce the power of monoclonal antibodies as tools to interrogate structure-function relationships of assembly-line PKSs.

\* Author to whom correspondence should be addressed: khosla@stanford.edu.

Supporting Information

Supporting Figures and Tables as well as the materials and methods can be found in the Supporting Information. The Supporting Information is available free of charge on the ACS Publications website.

## Graphical Abstract



## INTRODUCTION

Common to the repertoire of bacterial, fungal, and plant biosynthetic enzymes, polyketide synthases (PKSs) are protein factories that synthesize structurally complex polyketides and related hybrid compounds. Analogous to fatty acid synthases (FASs), PKSs operate by condensing acyl-coenzyme A (acyl-CoA) derived building blocks and then further modifying their elongated products via reductive, dehydrative, and other chemistries. In the course of these enzymatic transformations, PKSs introduce structural diversity into their products, often asymmetrically.

Assembly-line PKSs comprise a particularly intriguing branch of this enzyme family, where individual catalytic activities are organized into multidomain units called “modules”. Each module of catalysts is responsible for one round of polyketide elongation and modification. For example, the 6-deoxyerythronolide B synthase (DEBS) from *Saccharopolyspora erythraea* consists of a loading module (LM) and six elongation modules (M1-M6) housed in three large homodimeric proteins. Taking propionyl-CoA (starter unit), (2*S*)-methylmalonyl-CoA (extender units), and NADPH building blocks, this 2.1 MDa multimodular assembly line synthesizes the 14-membered macrocyclic core of the antibiotic erythromycin<sup>1,2</sup>. The catalytic cycle of each DEBS module begins by its ketosynthase (KS) domain receiving the growing polyketide from an upstream module (entry translocation) while an acyltransferase (AT) domain transfers a (2*S*)-methylmalonyl extender unit from the acyl-CoA metabolite pool onto the acyl carrier protein (ACP, transacylation). The KS then catalyzes a decarboxylative Claisen-like condensation between the extender unit and growing acyl chain to afford an elongated, ACP-bound  $\beta$ -ketoacyl thioester (elongation), concomitant with shielding of the KS active site<sup>3</sup>. Stereospecific reductive and dehydrative domains, such as ketoreductases (KR), dehydratases (DH), and enoylreductases (ER), function to modify the  $\alpha$ - and  $\beta$ -positions following elongation<sup>2,4</sup>. The product is either passed to a downstream module (exit translocation) or the full-length, linear intermediate is released by the terminal thioesterase (TE) domain through macrocyclization<sup>5</sup>; in both cases, reopening the KS active site and resetting the catalytic cycle<sup>3</sup>.

Since its discovery in the early 1990s, genetic and bio-chemical studies have illuminated the functions of the entire suite of DEBS catalytic domains, empowering engineered biosynthesis of 6-deoxyerythronolide B analogs<sup>6-8</sup>.

High-resolution X-ray or solution structures of representatives for each type of protein domain found in DEBS are now available<sup>4,9</sup>, and associated mechanistic studies have laid

the foundation for understanding the molecular logic of assembly-line PKSs<sup>10</sup>. A significant gap remains, however, in our ability to describe at a structural level how successive modules communicate with each other. In part, this is due to the intrinsically flexible ACP domain, which shuttles tethered polyketide intermediates to each catalytic domain of its own module and to the KS domain of the downstream module. Covalent crosslinking strategies have been deployed to capture these transient interactions between the ACP and its partner catalytic domains<sup>11–15</sup>; however, the only structures of intact assembly-line PKS modules come from negative stain analysis of the apratoxin loading module<sup>16</sup> and cryogenic electron microscopy (cryo-EM) studies of the DEBS-orthologous pikromycin synthase module<sup>5,17,18</sup>. In the latter examples, pseudo-atomic models were built by fitting high-resolution crystal structures of isolated DEBS domains into low-resolution (7.3 – 12.5 Å) electron potential maps. The cryo-EM models revealed a surprising “arched” structure in contrast to “extended” models predicted from X-ray crystallography of KS-AT didomains and size exclusion chromatography - small angle X-ray scattering (SEC-SAXS) analysis of intact modules and bimodules<sup>19,20</sup>. There remains a strong need for tools that can enable high-resolution structural analysis of intact modules at individual stages of their catalytic cycles.

Our lab previously characterized two fragment antibodies (F<sub>ab</sub>s; 1B2 and 3A6) derived from a large ( $3.7 \times 10^{10}$ ), phage-displayed human naïve antibody library. Antibodies 1B2 and 3A6 bind with high-affinity to the KS-AT didomain of DEBS M3 and the TE domain of DEBS M6, respectively (Fig. 1A). In both cases, co-crystal structures were obtained of the F<sub>ab</sub> and domain partner complexes, affording insights into the molecular details of antibody recognition<sup>20,21</sup>. The structure of 1B2 in complex with the KS-AT didomain from M3 recapitulated the previously observed extended conformation<sup>22–24</sup>. Kinetic analyses measured comparable  $k_{\text{cat}}$  and  $K_{\text{M}}$  values of M3 in the presence and absence of 1B2, suggesting the extended conformation is catalytically competent for the essential rate-limiting reactions (i.e., entry translocation and elongation). Further support for the catalytic relevance of the extended model came from SEC-SAXS analysis of 1B2-bound M3 in distinct catalytic states<sup>20</sup>.

Motivated by the ability of F<sub>ab</sub>s to trap PKS modules and fragments thereof in well-defined conformations, we sought to identify additional antibodies that bind to the KR domain of DEBS M1 (KR1). Here we describe two such F<sub>ab</sub>s (1D10 and 2G10) and harness their similarities and differences to glean new insights into the catalytic cycles of assembly-line PKSs.

## RESULTS

### Antibodies 1D10 and 2G10 bind specifically to KR1 albeit with distinct cofactor dependencies

Borrowing methods from our selection strategy described previously<sup>25</sup>, we identified two new F<sub>ab</sub>s, 1D10 and 2G10, that bound specifically to DEBS M1 (Supporting Figs. S1A and S1B). Their epitopes were localized exclusively to KR1 via competitive enzyme-linked immunosorbent assay (ELISA) involving the excised domain alone (Supporting Fig. S1C). In the absence of NADPH or CoA, 1D10 and 2G10 bound tightly to the stand-alone KR1 domain with dissociation constants of  $2.7 \pm 1.1$  nM and  $1.8 \pm 1.1$  nM, respectively (Figs. 1B

and 1C). To interrogate the effects of cofactors on antibody binding to KR1, NADPH, or CoA were added to ELISA plates. Addition of 0.2 mM NADPH reduced 1D10 binding by ca. 10-fold, but 2G10 binding to KR1 was unaffected by NADPH (Figs. 1B and 1C). In neither case did the addition of CoA significantly affect antibody binding to the ketoreductase.

### Antibody 1D10 but not 2G10 inhibits the NADPH-dependent ketoreductase activity of KR1

KR1 ordinarily catalyzes the diastereospecific reduction of an ACP-bound  $\beta$ -ketoacyl diketide intermediate (Fig. 2A). To investigate whether antibody binding alters ketoreductase activity, KR1-mediated reduction of *trans*-1-decalone (T1D) was assayed (Supporting Fig. S2)<sup>26,27</sup> in the presence or absence of 1D10 and 2G10 (Fig. 2B). Dose-dependent inhibition by 1D10 was observed, whereas 2G10 had no detectable effect on KR1 activity. Notably, under our assay conditions, the concentration of 1D10 required to inhibit KR1 activity is markedly higher ( $IC_{50} \sim 10 \mu\text{M}$ ; Supporting Fig. S3) than the measured dissociation constant of KR1–1D10 binding. To gain further insight into this unusual inhibitory mechanism, a 4 $\times$  kinetic analysis was performed by varying both NADPH and 1D10 concentrations (Supporting Fig. S4). Our data suggest that 1D10 inhibition of KR1 activity is competitive with NADPH binding.

To investigate the potential relevance of these KR1-specific  $F_{abs}$  to structure-function analysis of assembly-line PKSs, we analyzed their influence on the activity of a truncated bimodular derivative of DEBS (DEBS 1+TE) that synthesizes triketide lactone **2** (Fig. 2C)<sup>28</sup>. Again, PKS turnover was inhibited by increasing concentrations of 1D10 but not 2G10. The inhibitory potencies of 1D10 against the stand-alone KR1 and DEBS1+TE were comparable, suggesting that KR1 activity became rate-limiting for the turnover of the assembly-line in the presence of this monoclonal antibody. (In the absence of 1D10, the rate-limiting step in the formation of **2** is most likely chain translocation<sup>28</sup>).

### Structures of the KR1–1D10 and KR1–2G10 complexes

To structurally characterize the molecular details of antibody binding and inhibition of KR1, we solved the co-crystal structures of the KR1–1D10 (2.79 Å) and KR1–2G10 (2.25 Å) complexes using a combination of molecular replacement and homology modeling (Supporting Methods and Table S1). As is apparent from the two structures, 1D10 and 2G10 bind to distinct and spatially separated epitopes on the KR1 surface (Fig. 3A). In line with the observation that 1D10 competitively inhibits NADPH binding to the active site of KR1, the antibody directly overlays a portion of the NADP(H) binding site (near the 2'-phosphoadenosyl moiety) and adjacent to the putative acyl-ACP site (Fig. 3A). In contrast, 2G10 binds remotely from either binding site, consistent with its lack of inhibition (Fig. 3A). Notably, a loop in the light chain of 1D10 (Ser108 - Leu113) is situated in direct conflict with the modeled  $\text{NADP}^+$ , derived from superposition of the previously solved KR1-NADP<sup>+</sup> structure<sup>29</sup>; atomic overlap is observed between Ser110 ( $C_{\beta}$ ) and the 2'-phosphate of NADPH ( $O_{1X}$ ). Ser110 also appears in hydrogen bonding proximity to Ser1699 (KR1), disrupting a hydrogen bond that otherwise forms between Ser1699 and the 2'-phosphate of NADPH (Fig. 3A). This is likely a critical interaction for KR1, given the generally strict

specificity of anabolic enzymes for NADPH over NADH<sup>30,31</sup>. Taken together, our structural observations are in agreement with a competitive mode of 1D10 inhibition.

Overall, the previously solved KR1-NADP<sup>+</sup> structure<sup>29</sup> superposes well onto the KR1-F<sub>ab</sub> structures with no major backbone alterations (average RMSD = 0.705 Å over 2595 atoms), aside from one divergent loop fragment (Leu1756 - Thr1763) arising due to crystal packing interactions in the KR1-2G10 structure (Supporting Fig. S5). Key protein-protein interactions stabilizing the KR1-1D10 interface include electrostatic interactions between Arg1771(KR1) - Asp106 (1D10 heavy chain) and Arg1774(KR1) - Asp67(1D10 light chain) as well as hydrogen bonds between Thr1763 (KR1) - Ser33 (1D10 heavy chain) and Arg1768 (KR1) - Ser33 (1D10 heavy chain backbone; Fig. 3B). The KR1-2G10 interface is fortified by similar interactions; i.e., salt bridges between Arg1719 (KR1) - Asp56 (2G10 heavy chain) and Asp1742 (KR1) - Arg49 (2G10 light chain) and a hydrogen bond between Asp1743 (KR1) and Tyr61 (2G10 heavy chain). A hydrophobic wedge featuring Met106 (2G10 heavy chain) surrounded by KR1 residues Leu1694, Leu1736, and Ile1740 further stabilizes the KR1-2G10 interface (Fig. 3C).

To approximate how 1D10 and 2G10 might bind to KR1 in its modular context, we superposed the KR1-F<sub>ab</sub> structures onto the arched and extended models of a homodimeric, assembly-line PKS module (i.e., two symmetry-related copies of KR1-F<sub>ab</sub> per PKS homodimer; Supporting Fig. S6). Inspection of the SEC-SAXS derived model of DEBS M3+TE superposed with the KR1-F<sub>ab</sub> structures reveals no obvious clash between the two F<sub>ab</sub> subunits, consistent with their ability to bind simultaneously to a module in the extended conformation<sup>19</sup>. Conversely, significant overlap was observed between symmetry-related copies of 1D10 (but not 2G10) after superposition of the KR1-F<sub>ab</sub> structures onto the cryo-EM-derived arched model of pikromycin synthase module 5<sup>17,18</sup>. Thus, if a symmetric arched conformation were required during the DEBS catalytic cycle, it is likely that 1D10 binding would pose some inhibition to its turnover rate. To the contrary, we did not observe a corresponding increase in 1D10 inhibition after switching from free-standing KR1 reactions to bimodular DEBS reactions (Fig. 2B and 2C). We therefore posit, on the basis of these data, that 1D10 exerts its inhibition solely through competition for the NADPH binding site of KR1, not by influencing modular dynamics, and the conformation of M1 during ketoreduction more adequately fits the extended model of an assembly line PKS module.

### A chimeric PKS module derived from structurally defined enzymatic domains of DEBS

Earlier work from our laboratories highlighted the utility of size exclusion chromatography coupled with small angle X-ray scattering (SEC-SAXS) for low-resolution structural analysis of F<sub>ab</sub>-bound homodimeric PKS modules under catalytically relevant conditions<sup>20</sup>. We therefore sought to engineer a PKS module that satisfies the following criteria: (i) it is well-folded and has catalytic integrity; (ii) it is comprised exclusively of structurally characterized enzymatic domains; and (iii) it harbors epitopes for all DEBS-specific F<sub>ab</sub>s characterized to date. A chimeric module was engineered, comprising of the KS-AT didomain of M3 (which binds antibody 1B2), the KR domain of M1 (which binds antibodies 1D10 and 2G10), and the TE domain of M6 (which binds antibody 3A6). The design

specifications and sequence of this chimeric module are detailed in the Supporting Information. This hybrid module, abbreviated hereafter as M3/1+TE, was expressed as a C-terminally His<sub>6</sub>-tagged protein in *E. coli* and purified to homogeneity. Size-exclusion chromatography (SEC) verified that the protein was well-folded; its retention time was consistent with a 375 kDa homodimer (Supporting Fig. S7). The catalytic activity of purified M3/1+TE was compared to that of M3+TE in the context of a trimodular PKS (Figs. 1A and 4A). The rate of NADPH consumption was comparable in both cases (Fig. 4B), revealing that M3/1+TE was catalytically competent. The product of each reaction was confirmed by subjecting a methanol extract to analysis by liquid chromatography mass spectrometry (LC-MS). In both cases, the tetraketide ketolactone product **1** was observed (Fig. 4C), suggesting that KR1 was unable to compete with the TE domain for the  $\beta$ -ketoacyl-tetraketide intermediate. To verify activity of the KR1 domain in this chimeric module, M3/1+TE was tested in the T1D reduction assay described above. As seen in Supporting Figure S9, the enzyme retains its intrinsic ketoreductase activity.

### SEC-SAXS analysis of chimeric M3/1+TE bound to 1B2 and 1D10

Encouraged by the data highlighting the structural and functional integrity of M3/1+TE, we tested whether antibodies 1B2, 1D10, and 2G10 bind to M3/1+TE. Co-incubation of M3/1+TE with individual antibodies led to co-elution of each mixture of proteins on a SEC column with decreased retention time relative to either protein alone (Supporting Fig. S10). We therefore analyzed the complexes by tandem SEC-SAXS using similar methods as previously described (Supporting Methods)<sup>19,20</sup>. The 1B2-M3/1+TE and 1D10-M3/1+TE samples appeared monodisperse by peak profile and Guinier analyses, whereas corresponding scattering data from 2G10-M3/1+TE were indicative of non-uniformity, possibly due to aggregation and/or partial F<sub>ab</sub> dissociation (Supporting Table S2). Scattering curves from the former two samples were compared with simulated curves of the 1B2- and 1D10-bound models of an arched or extended PKS module. To account for the missing TE domain in the cryo-EM arched model<sup>17,18</sup>, we made two different TE modifications to the arched model: one (arched+TE model 1) featuring manual placement of the TE such that the ACP and TE domain termini are in the expected proximity for a continuous  $\alpha$ -helix and 8-residue spacer, and another (arched+TE model 2) where the TE was docked into the KR/ACP interface (Supporting Fig. S11)<sup>5</sup>. (Placement of the crystallographically observed dimeric TE near the ACP C-termini significantly occludes the 1D10 binding site<sup>5</sup>.) In all cases, experimental curves mapped more accurately onto predicted curves from the extended models ( $\chi^2_{1B2} = 1.93$ ,  $\chi^2_{1D10} = 5.29$ ) than those of the arched models ( $\chi^2_{1B2} = 8.49 - 12.64$ ,  $\chi^2_{1D10} = 18.14 - 30.42$ ; Fig. 5A,B; Supporting Figs. S12–S14 and Tables S2–S3)<sup>32</sup>. Given the resolution limitations of SAXS, we also considered the possibility that the F<sub>ab</sub>-M3/1+TE SAXS analytes correspond to singly F<sub>ab</sub>-bound modules. The predicted curves corresponding to models lacking one of the two symmetry-related F<sub>ab</sub> heterodimers also resulted in better alignment with the extended conformation model (Supporting Table S4).

## DISCUSSION

As with other complex protein systems, antibody fragments (F<sub>abs</sub>) are proving to be invaluable structural probes of assembly-line PKSs. Two F<sub>abs</sub>, 1D10 and 2G10, were

isolated and characterized as specifically recognizing the KR domain of DEBS module 1. Both antibodies bound KR1 with high affinity, albeit with different cofactor dependencies. F<sub>ab</sub> inhibition studies featuring stand-alone KR1 showed that 1D10 inhibited competitively through the NADPH binding site, whereas KR1 activity was unaffected by 2G10. Co-crystal structures uncovered the molecular basis for these differences. In particular, a loop in the 1D10 light-chain (i.e., Ser108-Leu113) bound in direct clash with the 2'-phosphate of NADP(H), while 2G10 bound nearly orthogonal to 1D10 and distal to the NADP(H) and acyl-ACP binding sites. We asked whether these F<sub>abs</sub> might serve as probes of modular dynamics of DEBS by testing their effects on the solution activity of a DEBS bimodule. After observing comparable F<sub>ab</sub> inhibitory effects in both the stand-alone and module-embedded KR1 contexts, we reasoned that F<sub>ab</sub> binding to DEBS module 1 should be compatible with conformational changes and protein-protein interactions that are otherwise absent in stand-alone KR1 reactions. Superposing each KR1-F<sub>ab</sub> co-crystal structure onto the arched and extended models of assembly-line PKS modules revealed significant overlap in 1D10 subunits in the arched model, running counter to expectations from our kinetic data. In other words, while an arched conformation was expected to confer increased vulnerability to 1D10 inhibition, this effect was not observed. Our data suggest that a PKS module harbors the extended conformation during ketoreduction. Further support came from SEC-SAXS analysis of a chimeric DEBS module, M3/1+TE, using methods from a prior report<sup>20</sup>. While our data do not definitively exclude the possibility of an arched or arched-like conformation existing at some point during the catalytic cycle, repeated observations of the extended conformation perhaps reflects its more ground-state nature compared to the arched conformation - thus far only observed by electron microscopy<sup>17,18</sup>. Future experiments aimed at characterizing discrete module conformations with higher spatial and temporal resolution will be required to parse out the functional relevancies of these, and possibly additional, conformations of a PKS module.

## Supplementary Material

Refer to Web version on PubMed Central for supplementary material.

## ACKNOWLEDGMENT

Use of the Stanford Synchrotron Radiation Lightsource, SLAC National Accelerator Laboratory, is supported by the U.S. Department of Energy, Office of Science, Office of Basic Energy Sciences under Contract No. DE-AC02-76SF00515. The SSRL Structural Molecular Biology Program is supported by the DOE Office of Biological and Environmental Research, and by the National Institutes of Health, National Institute of General Medical Sciences (including P41GM103393). The contents of this publication are solely the responsibility of the authors and do not necessarily represent the official views of NIGMS or NIH. The Pilatus detector at beamline 4-2 at SSRL was funded under National Institutes of Health Grant S10OD021512.

### Funding Sources

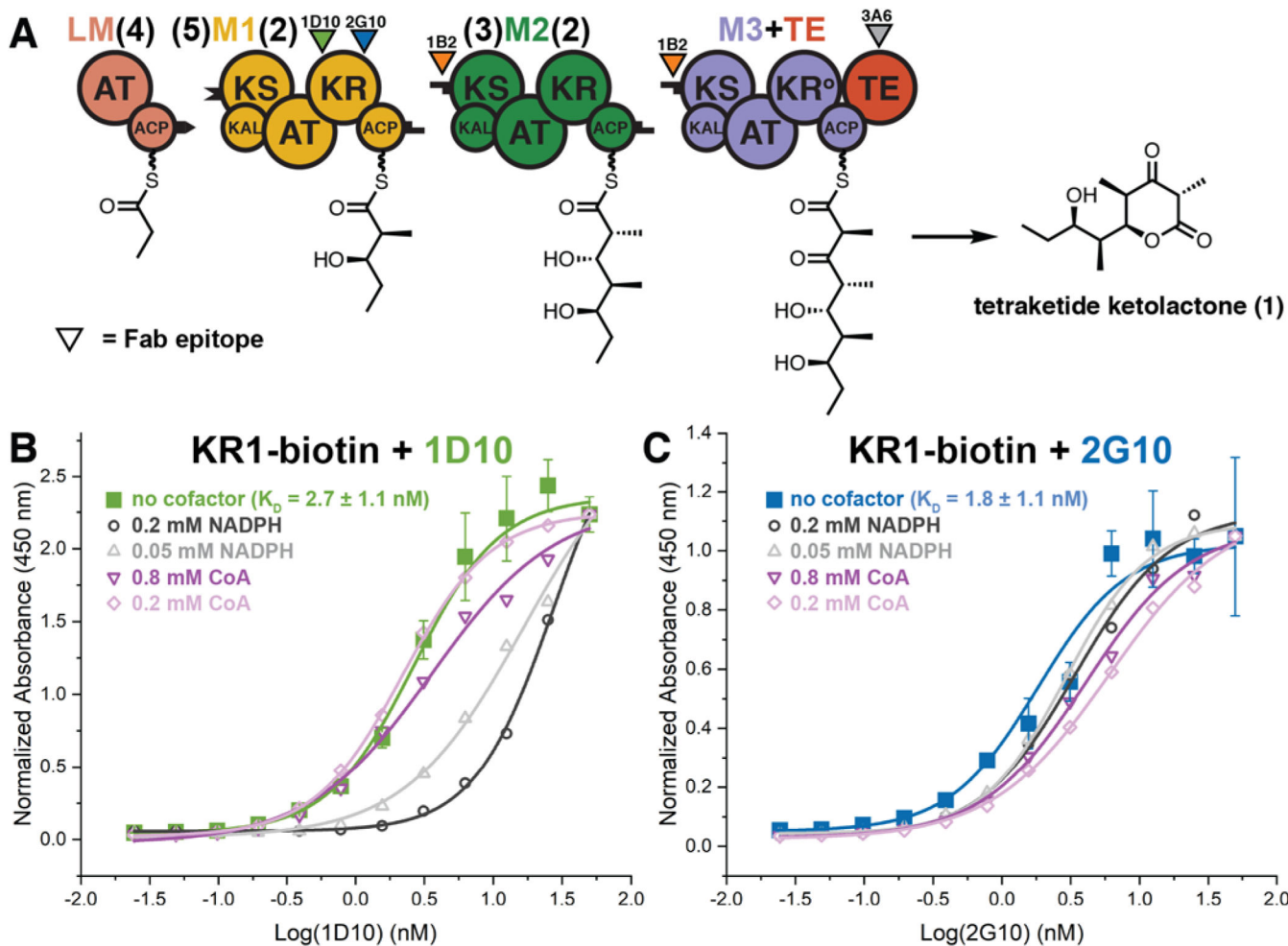
This research was supported by grants from the NIH (R01 GM087934 to C.K. and P50AI150476 to C.S.C.).

## REFERENCES

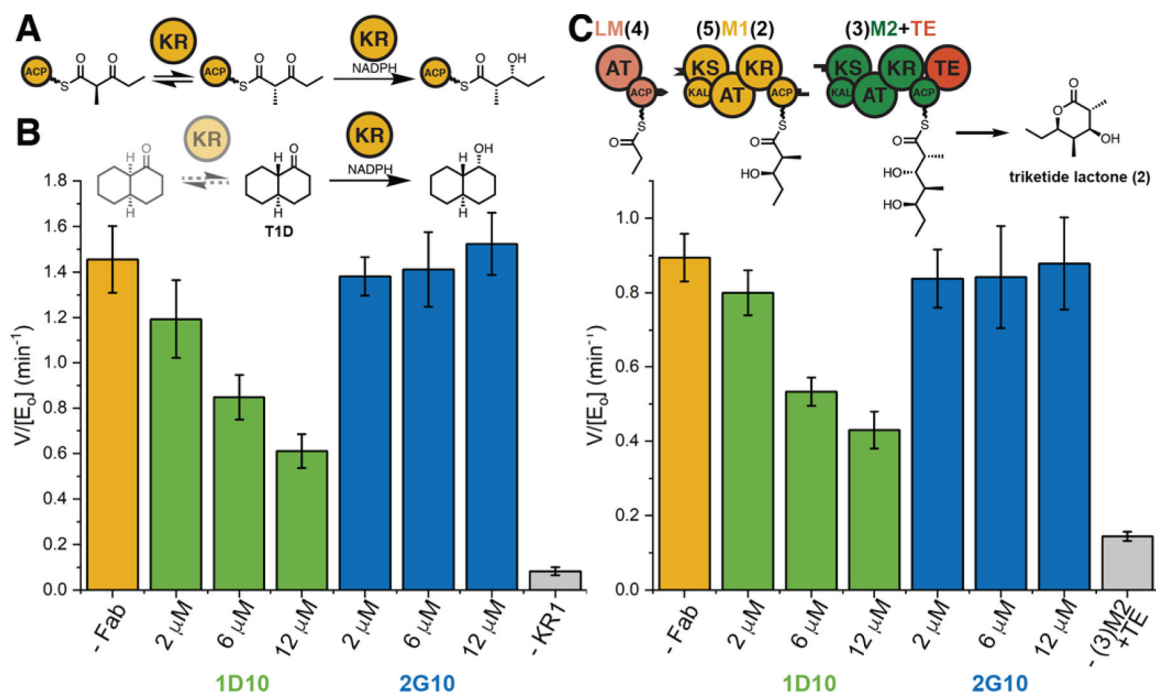
- (1). Khosla C; Tang Y; Chen AY; Schnarr NA; Cane DE Structure and Mechanism of the 6-Deoxyerythronolide B Synthase. *Annu. Rev. Biochem* 2007, 76 (1), 195–221. [PubMed: 17328673]

- (2). Robbins T; Liu Y-C; Cane DE; Khosla C Structure and Mechanism of Assembly Line Polyketide Synthases. *Curr. Opin. Struct. Biol* 2016, 41, 10–18. [PubMed: 27266330]
- (3). Lowry B; Li X; Robbins T; Cane DE; Khosla C A Turnstile Mechanism for the Controlled Growth of Biosynthetic Intermediates on Assembly Line Polyketide Synthases. *ACS Cent. Sci* 2016, 2 (1), 14–20. [PubMed: 26878060]
- (4). Keatinge-Clay AT The Structures of Type I Polyketide Synthases. *Nat. Prod. Rep* 2012, 29 (10), 1050–1073. [PubMed: 22858605]
- (5). Tsai SC; Miercke LJ; Krucinski J; Gokhale R; Chen JC; Foster PG; Cane DE; Khosla C; Stroud RM Crystal Structure of the Macrocyclic-Forming Thioesterase Domain of the Erythromycin Polyketide Synthase: Versatility from a Unique Substrate Channel. *Proc. Natl. Acad. Sci. U. S. A* 2001, 98 (26), 14808–14813. [PubMed: 11752428]
- (6). Donadio S; Staver MJ; McAlpine JB; Swanson SJ; Katz L Modular Organization of Genes Required for Complex Polyketide Biosynthesis. *Science* 1991, 252 (5006), 675 LP – 679. [PubMed: 2024119]
- (7). Cortes J; Haydock SF; Roberts GA; Bevitt DJ; Leadlay PF An Unusually Large Multifunctional Polypeptide in the Erythromycin-Producing Polyketide Synthase of *Saccharopolyspora erythraea*. *Nature* 1990, 348 (6297), 176–178. [PubMed: 2234082]
- (8). Walker MC; Thuronyi BW; Charkoudian LK; Lowry B; Khosla C; Chang MCY Expanding the Fluorine Chemistry of Living Systems Using Engineered Polyketide Synthase Pathways. *Science* 2013, 341 (6150), 1089 LP – 1094. [PubMed: 24009388]
- (9). Dodge GJ; Maloney FP; Smith JL Protein-Protein Interactions in “Cis-AT” Polyketide Synthases. *Nat. Prod. Rep* 2018, 35 (10), 1082–1096. [PubMed: 30188553]
- (10). Klaus M; Grininger M Engineering Strategies for Rational Polyketide Synthase Design. *Nat. Prod. Rep* 2018, 35 (10), 1070–1081. [PubMed: 29938731]
- (11). Milligan JC; Lee DJ; Jackson DR; Schaub AJ; Beld J; Barajas JF; Hale JJ; Luo R; Burkart MD; Tsai S-C Molecular Basis for Interactions between an Acyl Carrier Protein and a Ketosynthase. *Nat. Chem. Biol* 2019, 15 (7), 669–671. [PubMed: 31209348]
- (12). Nguyen C; Haushalter RW; Lee DJ; Markwick PRL; Bruegger J; Caldara-Festin G; Finzel K; Jackson DR; Ishikawa F; O’Dowd B; McCammon JA; Opella SJ; Tsai S-C; Burkart MD Trapping the Dynamic Acyl Carrier Protein in Fatty Acid Biosynthesis. *Nature* 2014, 505 (7483), 427–431. [PubMed: 24362570]
- (13). Miyanaga A; Iwasawa S; Shinohara Y; Kudo F; Eguchi T Structure-Based Analysis of the Molecular Interactions between Acyltransferase and Acyl Carrier Protein in Vicenistatin Biosynthesis. *Proc. Natl. Acad. Sci* 2016, 113 (7), 1802 LP – 1807. [PubMed: 26831085]
- (14). Miyanaga A; Ouchi R; Ishikawa F; Goto E; Tanabe G; Kudo F; Eguchi T Structural Basis of Protein-Protein Interactions between a Trans-Acting Acyltransferase and Acyl Carrier Protein in Polyketide Disorazole Biosynthesis. *J. Am. Chem. Soc* 2018, 140 (25), 7970–7978. [PubMed: 29870659]
- (15). Mindrebo JT; Patel A; Kim WE; Davis TD; Chen A; Bartholow TG; La Clair JJ; McCammon JA; Noel JP; Burkart MD Gating Mechanism of Elongating Beta-Ketoacyl-ACP Synthases. *Nat. Commun* 2020, 11 (1), 1727. [PubMed: 32265440]
- (16). Skiba MA; Sikkema AP; Moss NA; Lowell AN; Su M; Sturgis RM; Gerwick L; Gerwick WH; Sherman DH; Smith JL Biosynthesis of T-Butyl in Apratoxin A: Functional Analysis and Architecture of a PKS Loading Module. *ACS Chem. Biol* 2018, 13 (6), 1640–1650. [PubMed: 29701944]
- (17). Dutta S; Whicher JR; Hansen DA; Hale WA; Chemler JA; Congdon GR; Narayan ARH; Håkansson K; Sherman DH; Smith JL; Skiniotis G Structure of a Modular Polyketide Synthase. *Nature* 2014, 510, 512. [PubMed: 24965652]
- (18). Whicher JR; Dutta S; Hansen DA; Hale WA; Chemler JA; Dosey AM; Narayan ARH; Håkansson K; Sherman DH; Smith JL; Skiniotis G Structural Rearrangements of a Polyketide Synthase Module during Its Catalytic Cycle. *Nature* 2014, 510, 560. [PubMed: 24965656]
- (19). Edwards AL; Matsui T; Weiss TM; Khosla C Architectures of Whole-Module and Bimodular Proteins from the 6-Deoxyerythronolide B Synthase. *J. Mol. Biol* 2014, 426 (11), 2229–2245. [PubMed: 24704088]

- (20). Li X; Sevilano N; La Greca F; Deis L; Liu Y-C; Deller MC; Mathews II; Matsui T; Cane DE; Craik CS; Khosla C Structure-Function Analysis of the Extended Conformation of a Polyketide Synthase Module. *J. Am. Chem. Soc* 2018, 140 (21), 6518–6521. [PubMed: 29762030]
- (21). Li X; Sevilano N; La Greca F; Hsu J; Mathews II; Matsui T; Craik CS; Khosla C Discovery and Characterization of a Thioesterase-Specific Monoclonal Antibody That Recognizes the 6-Deoxyerythronolide B Synthase. *Biochemistry* 2018, 57 (43), 6201–6208. [PubMed: 30289692]
- (22). Tang Y; Kim C-Y; Mathews II; Cane DE; Khosla C The 2.7-Å Crystal Structure of a 194-KDa Homodimeric Fragment of the 6-Deoxyerythronolide B Synthase. *Proc. Natl. Acad. Sci* 2006, 103 (30), 11124 LP – 11129. [PubMed: 16844787]
- (23). Tang Y; Chen AY; Kim C-Y; Cane DE; Khosla C Structural and Mechanistic Analysis of Protein Interactions in Module 3 of the 6-Deoxyerythronolide B Synthase. *Chem. Biol* 2007, 14 (8), 931–943. [PubMed: 17719492]
- (24). Whicher JR; Smaga SS; Hansen DA; Brown WC; Gerwick WH; Sherman DH; Smith JL Cyanobacterial Polyketide Synthase Docking Domains: A Tool for Engineering Natural Product Biosynthesis. *Chem. Biol* 2013, 20 (11), 1340–1351. [PubMed: 24183970]
- (25). Kim J; Stroud RM; Craik CS Rapid Identification of Recombinant Fabs That Bind to Membrane Proteins. *Methods* 2011, 55 (4), 303–309. [PubMed: 21958987]
- (26). Ostrowski MP; Cane DE; Khosla C Recognition of Acyl Carrier Proteins by Ketoreductases in Assembly Line Polyketide Synthases. *J. Antibiot. (Tokyo)* 2016, 69 (7), 507–510. [PubMed: 27118242]
- (27). Ostergaard LH; Kellenberger L; Cortes J; Roddis MP; Deacon M; Staunton J; Leadlay PF Stereochemistry of Catalysis by the Ketoreductase Activity in the First Extension Module of the Erythromycin Polyketide Synthase. *Biochemistry* 2002, 41 (8), 2719–2726. [PubMed: 11851419]
- (28). Lowry B; Robbins T; Weng C-H; O'Brien RV; Cane DE; Khosla C In Vitro Reconstitution and Analysis of the 6-Deoxyerythronolide B Synthase. *J. Am. Chem. Soc* 2013, 135 (45), 16809–16812. [PubMed: 24161212]
- (29). Keatinge-Clay AT; Stroud RM The Structure of a Ketoreductase Determines the Organization of the Beta-Carbon Processing Enzymes of Modular Polyketide Synthases. *Structure* 2006, 14 (4), 737–748. [PubMed: 16564177]
- (30). Agledal L; Niere M; Ziegler M The Phosphate Makes a Difference: Cellular Functions of NADP. *Redox Rep.* 2010, 15 (1), 2–10. [PubMed: 20196923]
- (31). Kharel MK; Pahari P; Shaaban KA; Wang G; Morris C; Rohr J Elucidation of Post-PKS Tailoring Steps Involved in Landomycin Biosynthesis. *Org. Biomol. Chem* 2012, 10 (21), 4256–4265. [PubMed: 22454092]
- (32). Svergun D; Barberato C; Koch MHJ CRY SOL - a Program to Evaluate X-Ray Solution Scattering of Biological Macromolecules from Atomic Coordinates. *J. Appl. Crystallogr* 1995, 28 (6), 768–773.

**Figure 1.**

(A) Biosynthesis of a tetraketide ketolactone (**1**) by a truncated trimodular derivative of DEBS. Fab epitopes are shown as triangles (KAL = KS-AT linker, KR<sup>o</sup> = redox-inactive KR). Parenthetical numbers refer to N- and C-terminal docking domains from M2-M5<sup>28</sup>. (B, C) ELISA analysis of binding of 1D10 and 2G10 to biotinylated KR1 in the presence or absence of cofactors. The 1D10 and 2G10 heavy chains harbor C-terminal FLAG and Myc tags, respectively, enabling their detection by antibodies conjugated to horseradish peroxidase (Supplementary Methods). Data points corresponding to the “no cofactor” controls contain errors bars reflecting the standard deviations of three replicate measurements. All other data points correspond to single measurements.

**Figure 2.**

(A) Native reaction of KR1 whereby ACP1 bound diketide is epimerized then diastereospecifically reduced. (B) Influence of  $F_{\text{abs}}$  1D10 and 2G10 on the KR1-mediated reduction of the model substrate, *trans*-1-decalone (T1D,  $n=3$ ). (C) Influence of  $F_{\text{abs}}$  1D10 and 2G10 on the activity of a reconstituted DEBS bimodule producing the triketide lactone product (**2**,  $n=3$ ). Parenthetical numbers refer to DEBS N- and C-terminal docking domains from M2-M5<sup>28</sup>. Error bars reflect the standard deviations of three replicate measurements.

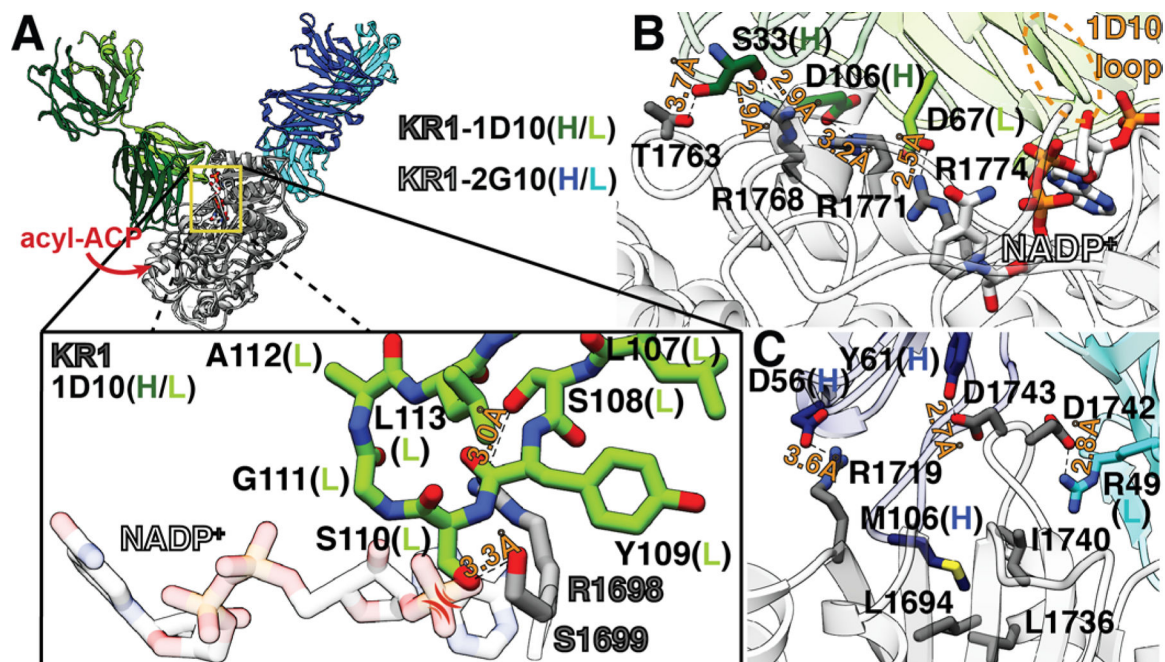


**Figure 3.**

(A) Macroscopic view of superposed KR1–1D10 (2.79 Å, PDB 6WH9) and KR1–2G10 (2.25 Å, PDB 6W7S) co-crystal structures (heavy “H” and light “L” chains are color coded). Boxed in yellow and expanded is the NADP(H) binding site with NADP<sup>+</sup> modeled via the previously solved KR1-NADP<sup>+</sup> structure (PDB 2FR0)<sup>29</sup> to highlight the clash between the 1D10 loop and 2'-phosphate of NADP(H). Close-up views of key interactions at the (B) KR1–1D10 (with modeled NADP<sup>+</sup>) and (C) KR1–2G10 interfaces (1D10 loop shown in the bottom of panel A is circled in dotted yellow).

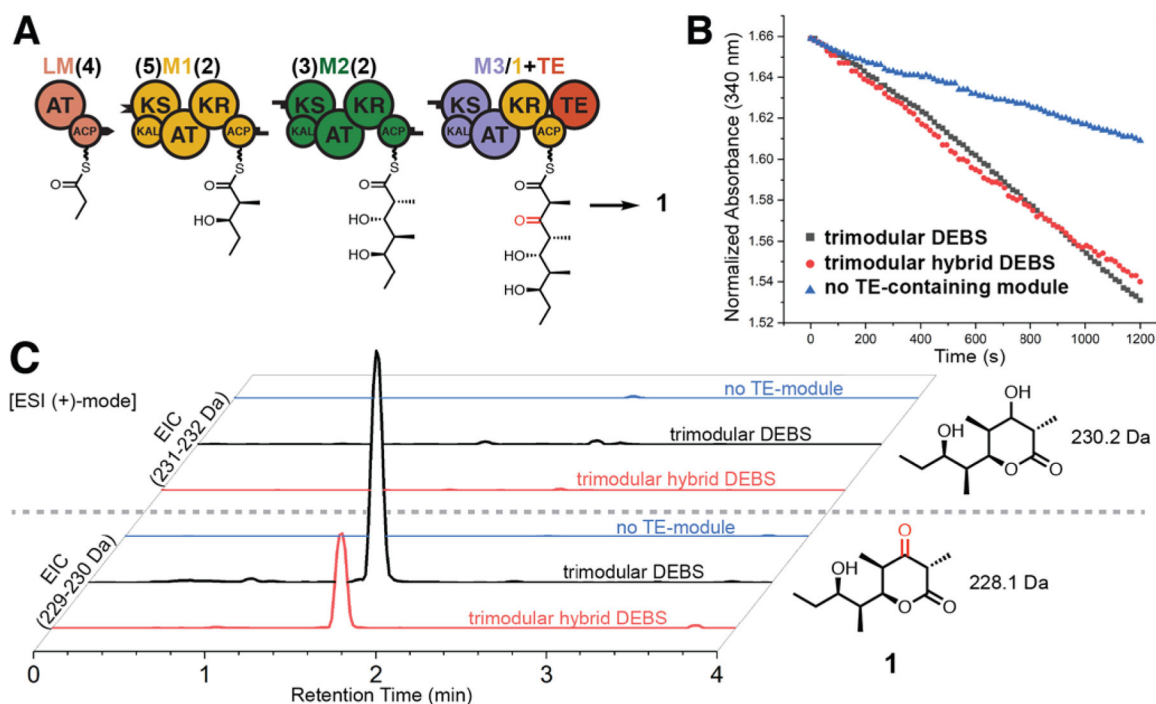


**Figure 4.**

(A) Reconstituted trimodular derivative of DEBS featuring M3/1+TE produces **1**. (B) NADPH depletion in a reconstituted native trimodular DEBS (black squares), trimodular hybrid DEBS (red circles), or a control reaction lacking the terminal TE-containing module (blue triangles). See Supporting Methods for reaction details. Parenthetical numbers refer to DEBS N- and C-terminal docking domains from M2-M5<sup>28</sup>. (C) LC-MS analysis of trimodular (native or hybrid) DEBS reactions. Extracted ion chromatograms (EICs) from positive ion mode electrospray ionization (ESI) for 231–232 Da and 229–230 Da mass ranges, corresponding to the protonated tetraketide lactone and tetraketide ketolactone, respectively. Data were collected on an Agilent 6470 triple quadrupole mass spectrometer (Supporting Methods).

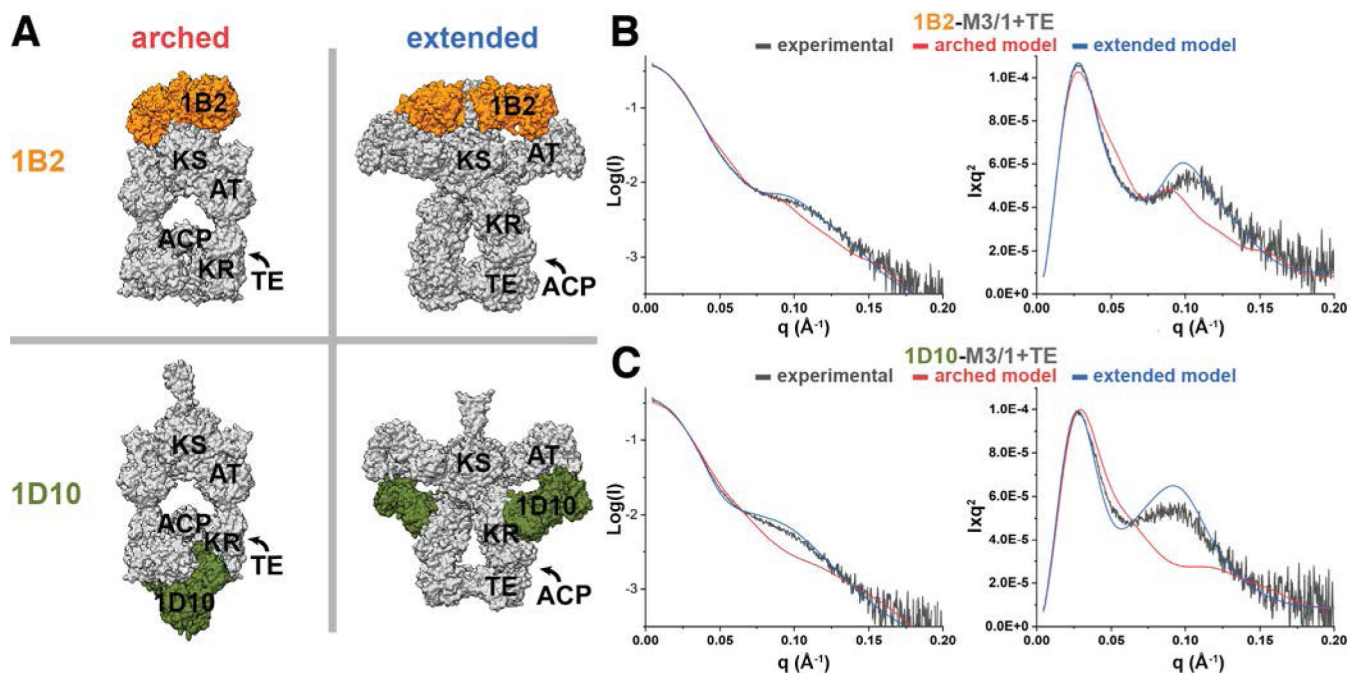


**Figure 5.** SEC-SAXS analysis of  $F_{ab}$ -bound M3/1+TE. (A) Arched (red)<sup>17,18</sup> and extended (blue)<sup>19</sup> models of an assembly-line PKS module bound to  $F_{ab}$ s 1B2 (orange)<sup>20</sup> and 1D10 (green). Domains of only one homodimer are labeled, for clarity. The arched models reflect the better fitting arched+TE model 1 (Supporting Fig. S11). (B,C) Log( $I$ ) vs.  $q$  (left) and Kratky (right) plots of the 1B2-M3/1+TE (panel B) and 1D10-M3/1+TE (panel C) experimental SEC-SAXS data (black traces) superposed with CRYSOLE-generated predicted curves for the arched (red traces) and extended models (blue traces) shown in panel A (Supporting Tables S2–S3)<sup>32</sup>.